3D quantitative elemental mapping using simultaneous proton induced X-ray emission tomography and scanning transmission ion microscopy tomography

Daniel Beasley *, Nicholas M. Spyrou

Department of Physics, Centre for Nuclear and Radiation Physics, School of Electronics and Physical Sciences, University of Surrey, Guildford GU2 7XH, UK

Abstract

A technique has been implemented that could produce sub-micron resolution quantitative elemental mapping of cells in an acceptable time frame. A new experimental set-up was installed to produce 3D quantitative elemental maps of biological samples by combining simultaneous proton induced X-ray emission tomography (PIXE-T), on/off-axis scanning transmission ion microscopy tomography (STIM-T) and Rutherford backscattering spectrometry (RBS). Combined with a high efficiency Si(Li) detector, 3D quantitative maps of Cl, S, Ca, K, Fe and Zn in a section of a hair were produced with an analytical time of 3 h.
© 2007 Elsevier B.V. All rights reserved.

1. Introduction

The combination of simultaneous on/off axis scanning transmission ion microscopy tomography (STIM-T) and proton induced X-ray emission tomography (PIXE-T) is a new method for micron-resolution quantitative 3D multi-elemental analysis. The equipment and software were installed and an experiment was performed to test the feasibility of this method in order to perform 3D micron-resolution analysis. Restrictions on the feasibility include time for analysis and limits of the accuracy of sample reconstruction especially as the sample is damaged during analysis.

Tomography has considerable advantages over 2D analysis. 2D analysis gives depth-averaged information while tomographic analysis allows the accurate localisation of

trace elements in microstructures without the need for sectioning therefore potentially damaging and exposing subcomponents to sources of contamination. Fine structures can be determined that can be easily masked by 2D analysis. Tomographic analysis does not only have applications to biomedical research but all fields where the composition of microstructures are important although this work is focused on biological samples.

STIM gives the ability of mapping samples by the measurement of proton energy loss passing through the sample. As the protons traverse the sample they lose energy, the amount of which is related to the electron density; with knowledge of the matrix (bulk) composition, the areal density can be determined. By measuring the energy loss and X-rays produced, trace element concentrations can be deduced. Rutherford scattering, where the energy and quantity of scattered protons are measured, can provide the bulk matrix composition, generally C, N and O for biological specimens which are difficult to detect by PIXE

---

especially with the low efficiency at low energies of our detector.

To further reduce the time required STIM-T is performed simultaneously with PIXE-T by using the on/off-axis configuration [1]. On-axis protons (taking a straight path through the sample) are scattered through a thin foil and detected by an offset detector. This also allows PIXE-T and STIM-T data sets to be mapped accurately, thus density correlates with elemental masses. This is the first time tomography has been performed using this configuration. Switching between the low and high currents greatly increases the time to perform the experiment. The beam would require optimising and the sample removed during this process.

The scattering foil allows protons to be measured that have travelled in a straight path through the sample using a detector in an off-axis position. Off-axis STIM measures protons that have scattered from a straight path therefore are not representative of the areal density along the path. This may also affect the number of protons detected, which is required to normalise to the charge. On-axis measurements are therefore more accurate but cannot be used alongside PIXE-analysis since PIXE requires a high current resulting in a prohibitive STIM count rate and detector damage.

X-ray production can be much more accurately determined by locating where in the sample the X-rays are generated. The correlation of elements can be more localised, in particular for structures within the sample such as the cell nucleus, without interference from extra-cellular material and the membrane, for example. Delicate and inhomogeneous samples can be analysed without sectioning, which may introduce contamination or structural damage. This is a great advantage when biological samples are to be analysed.

While ion beam tomography has been developed over a period of over 20 years [2], the complexities in reconstruction, the computing power required, and microprobe technology has hindered advances. Tomography experiments are still rare and the problems encountered have limited tomography measurements of cells to only a couple of experiments. In 1999, Michelet and Moretto [3] demonstrated impressive PIXE-T of a cultured human ovarian adenocarcinoma cell. However, with a basic reconstruction method only a limited number of major elements were identified due to the relatively inefficient experimental set-up. STIM-T of cartilage has been performed [4] and the data reconstructed using an iterative tomographic reconstruction method developed in Melbourne by Sakellariou [5], the Discrete Image Space Reconstruction Algorithm (DISRA). One major factor affecting the accuracy of PIXE data is the charge (number of protons) per pixel. To solve this problem, here the PIXE data were normalised to the STIM counts since there is no way of measuring the charge per pixel directly,

Due to the ease of preparation, relatively high levels of trace elements it was decided to perform a tomography measurement of hair. The levels of trace elements in hair are affected by the preparation method and performing tomography on hair may help resolve some issues regarding hair analysis without risk of contamination. PIXE-T and STIM-T of a section from a strand of hair was performed.

2. Tomographic reconstruction

The tomographic reconstruction is complicated by the non-linear physics involved in PIXE and STIM. 2D analysis only gives depth-averaged information; the non-linear energy loss of protons and the non-homogeneous distribution of trace elements mean that it is not possible to accurately determine the relation between X-ray yield and elemental mass in inhomogeneous samples. Hence the accuracy of 2D analysis, especially with intermediate to thick samples where energy loss may significantly affect the X-ray yield production at greater depths along the sample, can be significantly less than with 3D analysis. However the non-linear contribution of X-rays from voxels of same density and the discrete pixel-based data, along with technical inaccuracies, can violate the Radon Transform, the basis of tomographic reconstruction.

The DISRA program is the only current one for PIXE-T that takes into account X-ray attenuation in three dimensions allowing large detector areas without large assumptions in X-ray attenuation. Previous attempts assumed a point detector at a considerable distance or of a small area. Inhomogeneous samples can be analysed and attenuation calculated over many possible paths from the point of X-ray production to the detector.

Real experimental data are reconstructed using Filtered Back Projection (FBP). This is a poor method hence a computer model (phantom) of the sample is created based on the reconstructed data tomogram. The experiment is simulated. If the differences in the simulated projection data set and the experimental projection data set are low enough, the program returns the phantom. If not, the simulated data is reconstructed using FBP, and a comparison of the two tomograms is used to modify the phantom and the experiment is simulated again until the two data sets converge.

Accumulated noise, introduced by repeatedly applying the FBP, is reduced by allowing only values that fall into discretised bins, the size of which get smaller with each iteration. Thus, regions of similar value tend towards a joint value, so boundaries between regions are distinct and highlighted. This discrete version has been shown to be significantly more accurate than other methods employed for PIXE-T. For PIXE-T, the accuracy is in the region of 4–12% if the optimum number of projections is used and the STIM and PIXE beam spot size are equal.

3. Experimental set-up

The analysis took part at the University of Surrey Ion Beam Centre. Simon [6] has described the facilities in

depth. The tomographic equipment was designed for use in the microbeam line although this could be transferred to a new nanobeam line currently under construction. The microbeam can produce a beam brightness (or current density) of 1 pA μm^{-2} $mrad^{-2}$ MeV^{-1} for 2 MeV protons although this has been observed to be much higher [6].

A rotating flange is attached to the rear port which holds the Faraday cup (FC) and STIM detector. It can be rotated in order to place either the STIM detector or FC in the path of the beam. When the FC is in the path of the beam the STIM detector is in an off-axis position. The STIM detector is a relatively inexpensive Hamamatsu Si p-i-n photodiode. As protons can easily damage detectors, an inexpensive option is preferable. A 80 mm^2 Si(Li) detector was placed at 90°, as opposed to 315° for standard analysis, allowing it to be placed very close to the sample ensuring a high geometric efficiency. In standard 2D analysis a 3-axes Huntington PM-600 TRC Precision XYZ sample stage mounted onto the chamber lid is used. Sample plates sit at the end of a cold-finger and a container of liquid nitrogen cools the sample holder. There is a vertical displacement of 100 μm when the finger is cooled and the LN container requires cooling every 2 h or so [6]. It was for this reason, and as rotation of the cold finger may not be accurate to a sub-micron level due to the long axis, that a similar holder was not modified for tomography.

A collimator was produced by drilling a 1 mm hole in an aluminium plate. At the rear end of the collimator 150 nm gold leaf was brushed over the hole to act as a scattering foil. This was analysed by STIM to verify it's homogeneity and purity. It was found to be very homogeneous with the median channel being the same for all pixels and was found to contain approximately 2% copper.

By choosing gold the scattering cross-section is higher than carbon for example. A carbon film produced by a carbon arch and gold film produced by sputtering were tested but were found to have holes and be very fragile and often broke in the vacuum, so delaying analysis. Moreover gold leaf required just brushing of the foils on the plates which is much easier. Using this approach the STIM count rate can be adjusted more finely as the gradient of scattered protons is more pronounced.

The sample holder sits at the base of the chamber and consists of a stepper motor attached to a kinematic mount. A large copper plate is attached to the motor to assist as a heat sink – the motor is in a vacuum so heat is retained which may cause the sample to move up and down as the motor heats and cools. To prevent movement, the motor is only switched on when rotating, not when data is collected. A copper feedthrough can be attached to the copper plate using copper braid and the heat removed. The motor is controlled by a Parker Stepper drive and operated by software. The drive is programmed to turn the motor on, rotate a desired amount, and then to switch off and pause for the next projection to be taken. As the motor was only on for a very short amount of time, heat build up is negligible and no effect due to thermal expansion in the motor

was seen – the tip of a needle was observed and no change in the vertical profile recorded. To reduce the system dead time the motor was controlled using a separate computer to that used for data acquisition. A sample holder was built to sit at the bottom of the target chamber. A motor was placed on a kinematic mount. The conventional top-down 2D sample holder was used to hold the collimator and foils for STIM energy calibration.

The Si(Li) detector was placed at 90° to the beam, so increasing the geometric efficiency for PIXE at the expense of an increase in bremsstrahlung background. The pulse width was also decreased to increase the acquisition rate at the expense of energy resolution. However the peaks were very large relative to the background and distinct with few overlapping peaks and none for the elements that were tomographically reconstructed. To improve the reconstruction the sample was pre-irradiated. Changes in mass and morphology of biological samples prevent accurate reconstruction as the voxel size and relative positions move during the experiment. The majority of the elemental loss is O and H which are rapidly lost during PIXE analysis. The sample was irradiated until the rate of loss had decreased significantly. This was determined based upon previous experiments in the analysis of hair. The mass-loss was determined using RBS and attempts to correct for the loss made.

A Cu grid was scanned to determine the focused beam spot size and to check the calibration for the scanning amplifier. For greatest accuracy overlapping and gaps of pixels are minimised. A 900 nm aluminium foil and a 25 μm iron foil were used to calibrate the energy loss. These were characterised by STIM, PIXE and RBS beforehand as was the gold leaf used to scatter protons. Using SRIM [7] the energy loss was determined and the resulting STIM peaks were calibrated to the energy loss.

4. Analysis

A strand of untreated hair was inserted into a capillary that in turn was inserted into a hypodermic needle using superglue. The insertion was performed by hand under a microscope. This was in turn inserted into the shaft of the motor. The capillaries used were of approximately 100 μm internal diameter so that when the hair was inserted it rotated around the centre of mass as close as possible to reduce artefacts in the reconstruction. This worked reasonably well although several samples broke or were knocked when placed into the chamber. In Bordeaux [3] the sample holder can be adjusted and in Melbourne [5] a microstage was used, both of which improve the efficiency and accuracy of analysis by precise placement of the sample.

A 80 mm^2 Ortec Link Analytical Si(Li) detector was placed at 90° to the beam at a distance of 11 mm from the sample. A 1 mm-thick polythene funny filter with holes of an area of 1.06 mm^2 was placed over the detector. For RBS measurements a Si Surface Barrier detector was

placed at a distance of 60 mm and at an angle of 30° above the beam. For STIM measurements a collimator was placed approximately 10 mm behind the sample and protons were scattered by a gold foil at the back of the collimator A count rate of approximately 1000 cps was detected.

A 3 MeV proton beam with a 4.3 μm beam spot size and a current of 600–800 pA was used. It was intended originally that each pixel was dwelled upon for 1 s, although this was reduced to 0.8 s to reduce the experimental time. The total time for analysis was just over 3 h. Twenty two projections of 12 slices were taken over 360°. It was planned to take 25 projections but due to time constraints this was reduced to 22 projections. Fewer projections lead to a deterioration of the spatial resolution of the FBP reconstruction. The data acquisition software OMDAQ was used and DISRA was used to reconstruct the data. The STIM data was median filtered with a high and a low cut-off channel. As the counts per pixel were high, peaks in the spectra of individual pixels were clearly visible and the central channel matched the median values very well.

5. Data processing and normalisation

Event files produced by OMDAQ [8] were converted into the GeoPIXE [9] format to be read into DISRA and collated and converted into STIM and PIXE sinograms. The 2D maps were smoothed and centred around the central energy loss. Pixels containing no data were visible due mainly to the computer being occupied thus not acquiring data. To remove these the average of pixels either side were used to fill in gaps and smooth 'spikes' in the maps.

We have no charge/pixel measuring capability, so PIXE counts were normalised to STIM counts, assuming charge and STIM counts to be proportional. Each pixel in the experiment is normalised to the pixel with the highest pixel count.

$$\text{Normalised PIXE counts, } Cp_{x,y} = CpO_{x,y} \times \frac{Cs_{x,y}}{Cs_{MAX}}. \quad (1)$$

Here Cp is the normalised PIXE counts in a channel, CpO the original number of counts, and Cs is the STIM counts. The ratio of the normalised STIM counts and actual STIM counts is used to determine the new charge/pixel. However, this assumes the system deadtime has the same profile as the Si(Li) deadtime. Since the system deadtime largely depends on the computer processing time, it is close to the number of PIXE events.

$$\text{Charge, } Q = Q_0 \times \frac{\sum Cp_{x,y}}{\sum CpO_{x,y}}. \quad (2)$$

Here Q_0 is the original measured charge. The number of STIM counts, however, is dependent on the probability of scattering into the detector. The higher the energy, the lower the probability of scattering. However the loss of protons due to energy collimation has a much greater effect.

6. Results

Fig. 1 shows the results of the tomographic analysis. The elements S, Cl, K, Ca, Fe and Zn were reconstructed to produce 3D quantitative maps. The average density determined by STIM-T is approximately 0.8 g/cm³ although this varied per slice.

Twelve slices were analysed. A total volume of approximately 230,000 μm³ of hair weighing 0.2 μg was analysed. The total energy loss of the first projection, assuming an approximate homogeneous density and matrix composition, supports this.

A computer phantom of hair was created and the experiment simulated using DISRA to see if the distribution can be determined accurately with fewer projections, low concentrations etc. This was used to determine the contribution to the error from the reconstruction. Although voxels may have a very large error, regions are well defined. A separate paper will consider the experimental considerations. There are many sources of error and so although
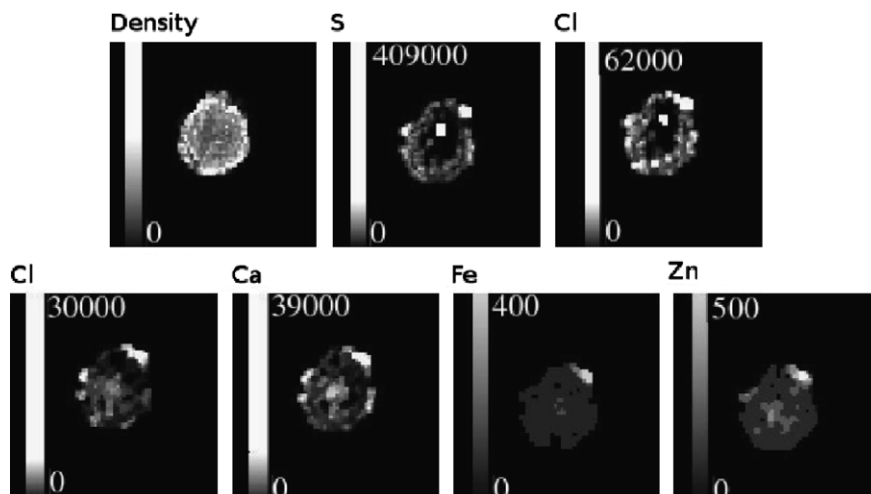

Fig. 1. Slice of hair produced using PIXE-T and STIM-T.

the experiment shows the technique to have great potential, considerable care must be taken. A brief summary of considerations are listed in the discussion.

7. Discussion

7.1. On/off-axis STIM and charge normalisation

The major problem with the use of gold foil was the contamination of gold and copper from it. Although the collimator was increased in length and the collimator moved backwards the foil was still visible by the Si(Li) detector. Moreover, protons scattered by the hair hit the aluminium collimator and these aluminium X-rays could be detected; the expected X-ray attenuation of aluminium was not very pronounced, suggesting the aluminium X-rays were not being produced in the hair but from the collimator. Both these contributions to the spectrum were identified earlier. Carbon was painted onto the collimator but it crumbled slightly in the vacuum. Hence the collimator was increased in thickness by using two sample plates.

The issue of STIM counts and beam broadening highlighted another issue – as the beam broadens in the sample a percentage of protons are lost by collimation. This is dependent on the degree of scattering. Hence the charge is underestimated in thicker regions and this is very dependent on the exact sample–collimator–foil distances. A SRIM simulation shows the percentage of protons lost through collimation as a function of energy loss with an estimate of 10 mm and 1 mm. By applying this to the STIM counts the charge-normalisation can be corrected for, but the exact geometry is not known.

7.2. Funny filters and efficiency

The filter used on the Si(Li) detector was a 1mm thick polyethylene filter. A number of holes in the filter allowed a certain percentage of lower-energy X-rays through. The given efficiency file with the filter did not correspond with the detected efficiency as for the same reason as the collimator for STIM. i.e. the geometry at 10 mm is not the same as for 25 mm. Moreover as the sample did not rotate perfectly around the centre, the distance from the sample to the filter varied by approximately 0.175 mm. Moreover, the filter/detector distance and so the exact geometry is unknown. Unless the exact efficiency at every distance is known there will be a source of error. It is therefore not advisable to use funny filters when the detector is close to the sample as was done here.

7.3. Beam damage correction

As can be seen by the maps in Fig. 2 the section of hair analysed shrunk. This is reflected by the change in matrix composition as determined by RBS. It has been assumed that after damage by the beam the major loss is due to oxygen and hydrogen. This is based upon previous analysis.
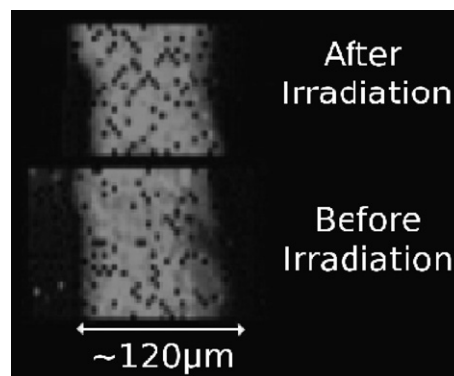

Fig. 2. STIM maps of hair showing the change in morphology after irradiation of PIXE-T.

The sample was therefore pre-irradiated. To ensure that the damage was even, the sample was rotated. Unfortunately on–off axis STIM measurements were not able to be reconstructed as the sample changed during the pre-irradiation. Also it was not possible to determine the loss from STIM measurements due to the change in sample morphology.

Approximately 0.2 μg of hair was analysed. However, during pre-irradiation slightly more than 12 slices were irradiated. Moreover, slices on either side of the 12 slices were occasionally irradiated during the experiment and this is not taken into account. Fig. 3 presents an approximate determination of the change in matrix composition using
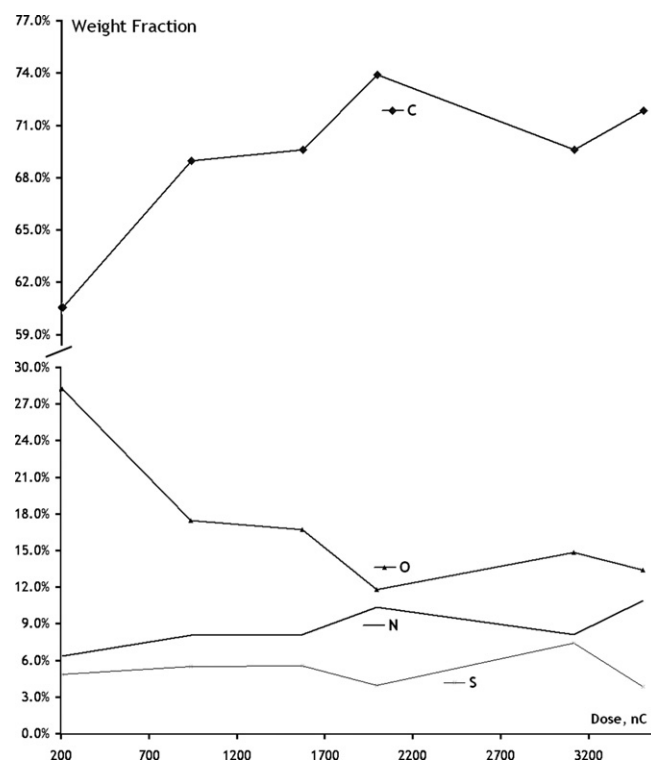

Fig. 3. RBS-determined change in matrix composition of approximately 0.2 μg of hair during irradiation of proton beam (600–800 pA, 1 s dwell-time).

RBS. A conservative estimate of dose per slice was assumed from previous analysis.

As can be seen, after the initial analysis, loss of matrix elements stabilises and trace elemental concentrations stabilise also after an initial rise. The problem of measuring mass loss using PIXE during tomography analysis is that light elements vary considerably depending on the orientation of the hair – if the oval hair is facing the detector many more counts are detected. Hence, this is one major benefit of tomography for such a sample. Assumptions in geometry often lead to major errors.

Beam blanking, where the beam is diverted when data are not being acquired, such as during detector dead time, would greatly reduce the damage to the sample and improve charge normalisation. This is now installed on the microbeam line.

7.4. Data acquisition

Although high speed scanning limits the damage to samples, as the hair is in a glass capillary which in turn is in a needle in a motor, the conductance path is complex. With the dose required for tomography it is inevitable that the sample will be damaged. Moreover with high speed scanning, mis-labelling of events often occurs. The beam was scanned across a metal plate and the gradient of counts differed depending on whether the scan was up or down.

The beam dwelled on each pixel for approximately 1 s, however the STIM and PIXE maps appeared patchy with empty pixels. The system deadtime is considerably higher for the PIXE and STIM than for detector deadtime. This is a major problem with certain data acquisition software – the deadtime is dependent on the computer processes.

If data is saved in batches, every 5 s or so the deadtime rises considerably. The maps were smoothed before processing.

To improve the efficiency of PIXE experiments, a more flexible beam scanner and data acquisition system would be highly desirable. As described above, STIM counts would not be counted when the beam is deflected so charge normalisation would be far more accurate. There is only one scan amplifier so the scan is always square. The magnets therefore had to be adjusted to create a beam of equal width and height and then the amplifier adjusted accordingly. This was a long procedure and compromised the spatial resolution and so the current density.

8. Conclusions

The potential of this technique is high. With an increase in beam current density available on completion of a new nanobeam facility, this will result in sub-micron resolution tomography on cells.

References

[1] D. Beasley, N.M. Spyrou, J. Radioanal. Nucl. Chem. 264 (2) (2005) 289.
[2] I. Akira, K. Hiroko, Nucl. Instr. and Meth. B 3 (1–3) (1984) 584.
[3] C. Michelet, Ph. Moretto, Nucl. Instr. and Meth. B 150 (1–4) (1999) 173.
[4] T. Reinert, U. Reibetanz, J. Vogt, T. Butz, A. Werner, W. Grunder, Nucl. Instr. and Meth. B 181 (1–4) (2001) 511.
[5] A. Sakellariou, D.N. Jamieson, G.J.F. Legge, Nucl. Instr. and Meth. B 181 (2001) 211.
[6] A. Simon, C. Jeynes, R.P. Webb, R. Finnis, Z. Tabatabaian, P.J. Sellin, M.B.H. Breese, D.F. Fellows, R. van den Broek, R.M. Gwilliam, Nucl. Instr. and Meth. B 219 (20) (2004) 405.
[7] J.F. Ziegler, Srim-2003, Nucl. Instr. and Meth. B 219 (2004) 1027.
[8] G.W. Grime, Nucl. Instr. and Meth. B 89 (1994) 223.
[9] S.H. Sie, W.L. Griffin, G.F. Suter, C.G. Ryan, D.R. Cousens, E. Clayton, Nucl. Instr. and Meth. B 47 (1990) 55.